CRACKING AND DEBONDING IN INTEGRATED MICROSTRUCTURES

X.H. LIU*, Z. SUO*, Q. MA** and H. FUJIMOTO**
* Mechanical and Aerospace Engineering & Princeton Materials Institute, Princeton University, Princeton, NJ 08544
** Components Research, Intel Corporation, Santa Clara, CA 95052

ABSTRACT

Internal stresses inevitably arise in integrated microstructures. This paper reviews a fracture mechanics approach to devising design rules to avert cracking. The smallness of the feature size permits a strategy different from that conventionally used to analyze the fracture of bulk materials. In an integrated microstructure, high tensile stress is localized in small regions. The elastic energy stored in each region scales with its volume. The surface energy associated with the creation of a crack scales with the surface area of the crack. Thermodynamics dictates that a flaw cannot grow if the stored elastic energy is lower than the created surface energy. Consequently, for a sufficiently small feature size, the volume-to-area ratio is small, and no flaw can grow. Our design rules do not depend on flaw size. They are deterministic, and rely on well-specified geometric and physical parameters. Furthermore, the stress singularity at corners does not cause any particular difficulty. As an example, the thermal misfit cracking in a multilevel interconnect test structure is investigated.

INTRODUCTION

In an integrated microstructure stresses arise from many origins. The deposition process can generate stress, known as intrinsic stress; for example, a chemical vapor deposited tungsten film has an intrinsic stress close to 1 GPa [1,2]. Upon cooling after the processing temperature, dissimilar materials undergo thermal contraction, leading to misfit stresses [3,4]. When a circuit is in use, the electric current can cause mass diffusion (i.e., electromigration); voids form where mass depletes, and stresses arise where mass accumulates [5-7]. In several instances, the stresses are known to cause cracking in brittle materials and debonding of interfaces. To reduce cost and increase yield, design rules are needed to avert cracking and debonding. The need is ever more imperative as the integrated microstructures become more complex, with new geometry and new materials.

Over the last decade the microelectronic industry has developed several basic capabilities concerning the problem. Stresses in simple structures, e.g., blanket films and parallel lines, can be measured with wafer curvatures and X-ray diffraction [1,3]. Raman spectroscopy has been used to measure local stresses induced in the underlying silicon [8]. Fracture energy of materials and interfaces have been measured from the simple structures [9-11]. The measurements provide material data, such as yield strength and intrinsic stress. Based on the data, one can develop finite element models to predict behaviors of more complex structures [1-4]. Such models have been successful in correlating measurements and calculations of average stresses in metals.

The finite element models, however, have not been used to predict cracking and debonding in integrated microstructures. Two basic difficulties exist. First, stresses are high, possibly singular at corners, and are sensitive to geometric details. Second, the strength of a brittle material is an ill-defined quantity. Consequently, it is unclear how the stresses generated by the finite element models can be used to predict cracking. To date no physically based design rules to avoid cracking in integrated microstructures have been established.

Mat. Res. Soc. Symp. Proc. Vol. 516 © 1998 Materials Research Society

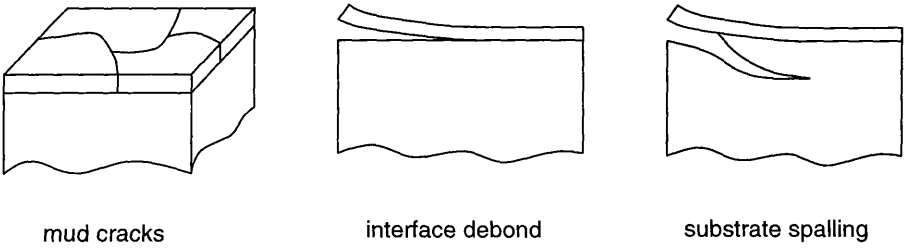

Figure 1. Basic cracking behaviors in a film-substrate system.

DESIGN RULES BASED ON FRACTURE MECHANICS

We propose an approach to devising design rules to avoid cracking. This section describes the basic concepts. The smallness of the feature size allows a particular approach, which is less appreciated but is well grounded within fracture mechanics. It has been developed to analyze cracking induced by thermal expansion misfit in systems containing small objects such as inclusions, fibers, and thin films [12-16]. In such a system, tensile stress is localized, so that the associated elastic energy is mainly stored in a volume comparable to that of the small object. When a crack forms, the system releases some elastic energy, but gains surface energy. Thermodynamics dictates that the crack should not form if the elastic energy released is less than the surface energy gained. The elastic energy scales with the volume, and the surface energy scales with the area. When the feature size is small, so is the volume-to-area ratio. Consequently, for a small enough feature size, the elastic energy stored in the system is insufficient to cause cracking. Under this condition, no flaw can grow, regardless its size, orientation, or location. This no-cracking condition is independent of the information of flaws. Nor does the singular stress field at a corner cause any particular concern: the tensile stress is high only in a small volume, and the total amount of elastic energy is finite.

The following examples will clarify various points. First consider a thin film on a much thicker substrate. The film is under a biaxial stress, but the substrate has negligible stress. For the present discussion assume that during cooling the film does not undergo inelastic deformation. The magnitude of the biaxial stress in the film, σ, can be written as

$$\sigma = \sigma_0 + \frac{E_f}{1-\nu_f}(\alpha_f - \alpha_s)(T_0 - T). \tag{1}$$

Here, σ_0 is the intrinsic stress developed at the processing temperature, E_f and υ_f are Young's modulus and Poisson's ratio of the film, α_f and α_s are the thermal expansion coefficients of the film and the substrate, T_0 is the deposition temperature, and T is the current temperature. Note that the thermal stress is independent of the film thickness. The intrinsic stress may depend on the film thickness; for simplicity, such dependence will be ignored in the following discussion. Thus, to a good approximation, the residual stress in the film is independent of the film thickness.

Common experience indicates that, everything else being equal, a thick film is more prone to cracking than a thin film. The phenomenon can be understood from an energetic consideration. Figure 1 illustrates representative cracking modes. The stress may cause mud cracks in the film, debonding along the interface, and spalling in the substrate. For all the cracking modes, the condition for no cracking or debonding takes the form [14,16]:

$$\beta \frac{\sigma^2 h}{E_f} < \Gamma . \tag{2}$$

Here h is the film thickness, Γ the fracture energy for the appropriate fracture path, β a dimensionless number to be determined from the appropriate elasticity solution. The film thickness h enters this comparison of elastic and surface energy, as will become evident below.

Consider the case of interface debonding. Compare the free energies of the two states of the film-substrate system: the bonded or the debonded state, Fig. 2. In the bonded state, the free energy consists of the elastic energy stored in the film and the interface energy:

$$\frac{(1-\nu_f)\sigma^2}{E_f} h + \gamma_{12} . \tag{3}$$

Debonding transforms the interface into two free surfaces. In the debonded state, the stress is relieved, and the free energy consists of the surface energy of the film and that of the substrate:

$$\gamma_1 + \gamma_2 . \tag{4}$$

The film cannot debond if the free energy is lower in the bonded state than in the debonded state. A comparison of (3) and (4) reproduces the general condition (2), with the identification,

$$\Gamma = \gamma_1 + \gamma_2 - \gamma_{12} , \tag{5}$$

and

$$\beta = 1 - \nu_f . \tag{6}$$

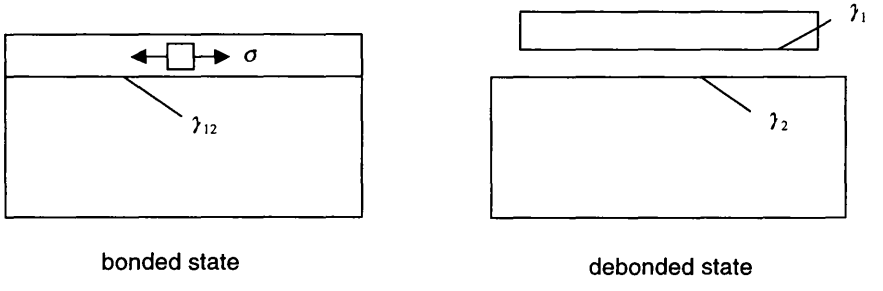

Figure 2. Two thermodynamic states: bonded and debonded film-substrate system.

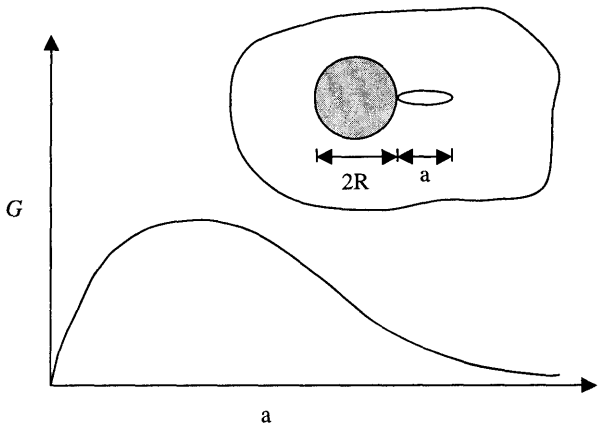

Figure 3. A cylinder embedded in a matrix.

In this example, the elastic energy is stored in the film. As the film becomes thinner, the amount of the elastic energy decreases but the change in the surface energy due to debonding remains the same. Consequently, when the film thickness is less than a critical value, the elastic energy is insufficient to cause debonding. This example is particularly simple because the change in elastic energy can be readily computed. In general, however, the elastic energy variation has to be computed by solving an elasticity boundary value problem. Analysis for various cracking modes in the film-substrate system has been summarized in [14,16].

The following example shows how the approach treats flaws. Figure 3 illustrates a long cylinder embedded in a matrix. The cylinder is under residual compression, and the matrix has a tensile hoop stress. Evidently, the stress in the matrix is non-uniform, high near the cylinder and vanishing far away. Whether the hoop stress will cause cracking depends on flaw characteristics: how large the flaw is and where it is. Such information is usually unavailable. Consequently, whether the matrix will crack is statistical. One can, however, set a deterministic design rule on the basis of the worst scenario. Imagine that we introduce flaws of different sizes in the matrix. Figure 3 sketches the elastic energy release rate, G, as a function of the flaw size, a. The energy release rate is small for very small flaws. For very large flaws, because the stress in the matrix decays far away from the cylinder, the energy release rate is also small. Consequently, the energy release rate reaches maximum, $G_{\max}$, for a flaw of intermediate size. For a cylinder of radius R under compressive stress σ, the maximum occurs at $a = R/2$ and $G_{\max} = 0.058(1-\nu^2)\sigma^2 R/E$; see reference [13]. If this maximum energy release rate is below the fracture energy of the matrix material, Γ, no flaw can grow. Thus, the no-cracking condition is

$$0.058(1-\nu^2)\sigma^2 R/E < \Gamma. \tag{7}$$

Note that this condition depends on well-defined parameters, and takes the similar form of equation (2). Everything else being equal, a cylinder of a large radius is more likely to cause matrix cracking than a cylinder of small radius.

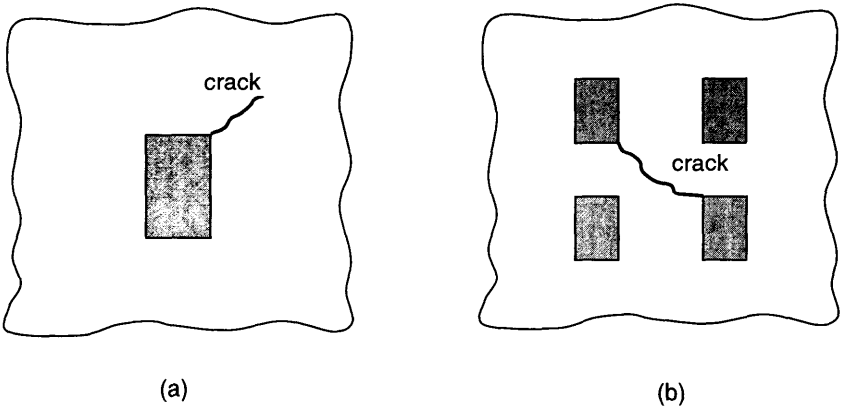

Figure 4. in an oxide matrix, the aluminum lines are under a pressure due to electromigration. This causes cracking in the dioxide matrix. (a) A crack emanates from a corner of an aluminum line. (b) A crack connects closely spaced aluminum lines.

For simplicity, we have assumed, in the above, that the elastic constants of the matrix and the cylinder are similar. The more general case has been treated in [15]. In an integrated microstructure, sharp corners are pervasive. For example, Fig. 4(a) illustrates the cross-section of an aluminum line embedded in a silicon dioxide matrix. The aluminum line is under compression, say, due to electromigration [7]. Near a corner, the stresses are expected to be very high and cannot be written in a simple analytical form as above for the cylindrical case. Nevertheless, the above approach is equally valid because the elastic energy stored is limited.

In the above example, the possible crack size is limited because the tensile stress decays rapidly in the radial direction. In an integrated microstructure, the materials in compression or of high toughness can also limit the crack size. For example, Fig. 4(b) illustrates closely spaced interconnects embedded in an oxide matrix. The residual compression in interconnects induces a large tensile stress in the matrix between them. The largest crack is set by the spacing between interconnects. If the elastic energy released by this largest crack is smaller than the surface energy, no flaw can grow to join the two interconnects. The spacing will be the length scale that enters the no-cracking condition (2), with various length ratios entering β.

A MULTILEVEL INTERCONNECT TEST STRUCTURE

In this section we consider a multilevel interconnect test structure (Fig. 5), and propose design rules to avoid cracking. The stack consists of three aluminum pads in a silicon dioxide matrix, all lying on a silicon substrate. This structure is known to crack in the trench between the aluminum pads. The reason is two folds. First, upon cooling, thermal expansion misfit induces a tensile stress in the oxide. Second, an unfortunate feature of the structure is that the volume of oxide under tensile stress is large, so that the amount of elastic energy that can be released by such a crack is large. One obvious solution is to change the geometry to reduce the volume of the oxide under tension.

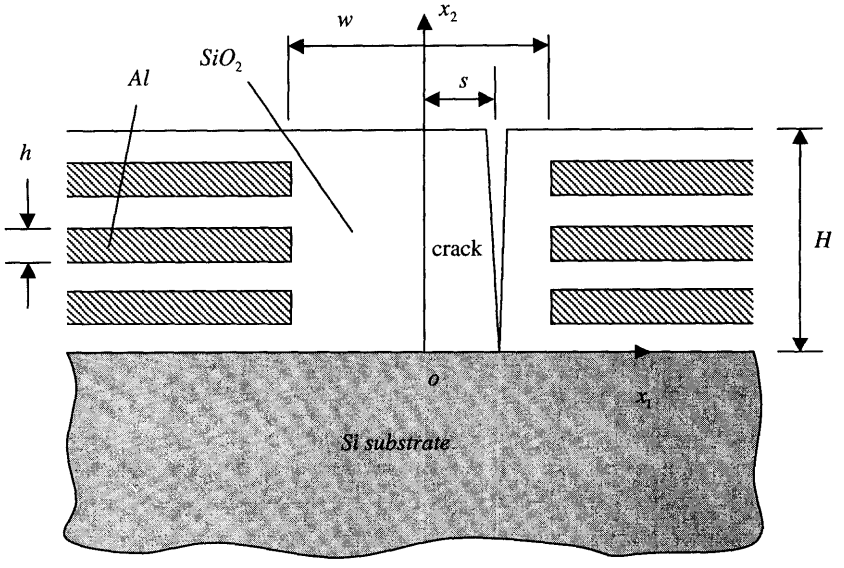

Figure 5. An integrated microstructure which is known to develop crack during processing.

A set of design rules are required that specify whether a given placement of the metal pads lead to cracking. The design rules should incorporate the physical properties of the metal and oxide, the thickness of the oxide, H, various length ratios, as well as the stacking sequence. In this structure the crack is confined in the oxide film, propagating in the x_3 direction which is perpendicular to x_1 and x_2 directions shown in the figure. This is one form of cracking, a tunneling crack. The geometry is well defined, so that detailed calculations can be performed and experiments to ascertain the validity of the approach can be designed.

Consider the stress in a blanket aluminum film on a silicon substrate due to thermal expansion. Before the film undergoes inelastic deformation, the stress in the film is

$$\sigma_{bf} = \frac{E_{\mathrm{Al}}}{1-\nu_{\mathrm{Al}}}(\alpha_{\mathrm{Al}} - \alpha_{\mathrm{Si}})\Delta T \,. \tag{8}$$

This stress prevails for the stress in the aluminum pads far away from the trench. We will use this stress to normalize the energy release rate. Here we assume that aluminum remains elastic, and consider the temperature drop to the point where aluminum starts to yield. The energy release rate takes the form

$$G = \beta \frac{\sigma_{bf}^2 H}{E_{\mathrm{Al}}} \,. \tag{9}$$

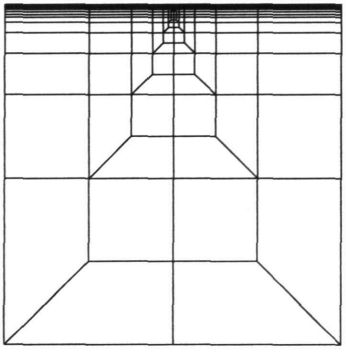

(a)

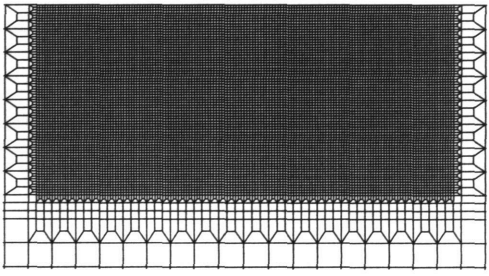

(b)

Figure 6. (a) Typical finite element mesh for tunneling crack. (b) refine mesh around the trench.

Here the number β, to be computed, depends on various dimensionless ratios, such as Poisson's ratios, Young's modulus ratios. Once the material constants are fixed, β is a function of the length ratios:

$$\beta\left(\frac{h}{H}, \frac{w}{H}\right). \tag{10}$$

Evidently, everything else being fixed, the smaller the aluminum pads thickness h, the smaller β. β also decreases as the trench width increases; because the stress in the oxide decreases when $w \to \infty$. Once the function β is computed, the no-cracking condition is

$$\beta \frac{\sigma_{bf}^2 H}{E_{\text{Al}}} < \Gamma_{\text{ox}}, \tag{11}$$

where Γ_{ox} is the fracture energy of the silicon dioxide. Again the condition takes the same form as (2).

The function β has to be computed using finite element methods. As an example of the calculation method, consider the tunneling crack in the middle of the trench, that is, $s = 0$ in Figure 5. First, the finite element method is used to analyze the elastic field in the structure without the crack, from which the stress component normal to the prospective crack, $\sigma(y)$, is obtained. Second, the finite element method is used to analyze the elastic field in the structure with the crack, from which the crack opening displacement, $\delta(y)$, is obtained. The elastic energy released due to the introduction of the crack is then [15],

$$G = \frac{1}{2H} \int_0^H \sigma(y)\, \delta(y)\, dy. \tag{12}$$

Table 1. Elastic modulus, Poisson's ratios and coefficient of thermal expansions [8]

Material	E (GPa)	ν	$\alpha\ (10^{-6}/^{\circ}\mathrm{K})$
Al	70	0.33	27.0
SiO_2	94	0.16	1.3
Si	130	0.28	3.4

From this energy release rate, one can extract the value of β. The calculations are repeated for various length ratios, h/H and w/H. The approach can be readily extended to the off-center cracking ($s \neq 0$).

A typical finite element mesh is shown in Figure 6(a). It consists of 15,349 nodes and 15,148 bilinear quadrilateral elements. The thickness and width of the substrate are about 400 times the film thickness. Around the trench the mesh is refined to resolve the stress concentration there, as shown in Figure 6(b). The elastic moduli, Poisson's ratios and coefficients of thermal expansion are fixed in all calculations; their values are listed in Table 1. The generalized plane strain conditions are assumed. We used the commercial code, ABAQUS, to compute the displacement and stress. The output was integrated numerically according to (2) to obtain the energy release rate.

Figure 7 shows the dimensionless β as a function of length ratios h/H and w/H for the tunneling crack at the middle of the trench. The energy release rate decreases significantly as the trench width w increases. Each curve for a given h/H is nearly a straight line. With everything else fixed the number β increases greatly as the aluminum pad thickness h increases. For a blanket film under a tensile residual stress on a substrate, β was found to be 1.976 [14]. This value was recovered in our calculations for $h/H = 1/3$.

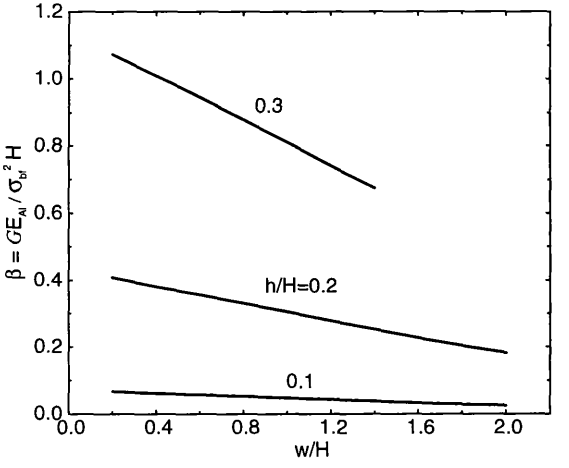

Figure 7. The dimensionless number β in the energy release rate (9) as a function of length ratios h/H and w/H.

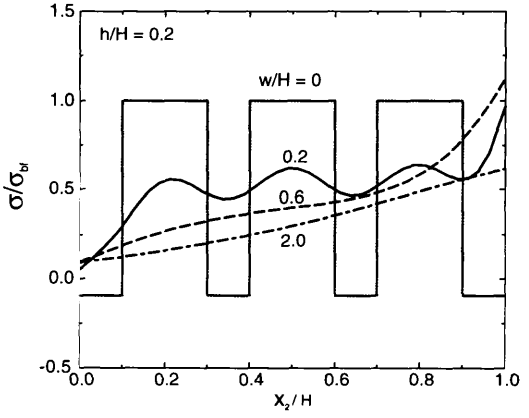

Figure 8. Variations of the normal stress on the middle plane of the trench ($x_1 = 0$) for various trench width ratio w/H with aluminum thickness fixed at $h/W = 0.2$. The ordinate is from the oxide/silicon interface ($x_2/H = 0$) to the oxide surface ($x_2/H = 1$).

Figure 8 shows the normal stress at the middle of the trench before tunneling crack arrives for h/H = 0.2. In the case of no trench (w/H = 0) a uniform stress arises within each material, tensile in the aluminum pads and compressive in the oxide. This is due to the large coefficient of thermal expansion (CTE) of Al and the small CTE of SiO_2 compared to the Si substrate. The stress fluctuation diminishes as the trench width increases. In spite of the

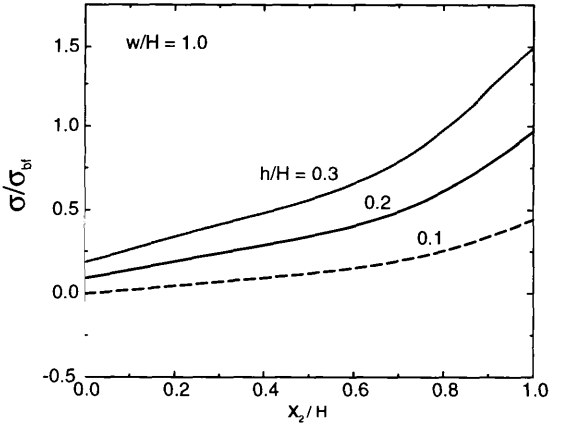

Figure 9. Variations of the normal stress on the middle plane of the trench ($x_1 = 0$) for various pad thickness ratio h/W with the trench width ratio fixed at $w/H = 1.0$.

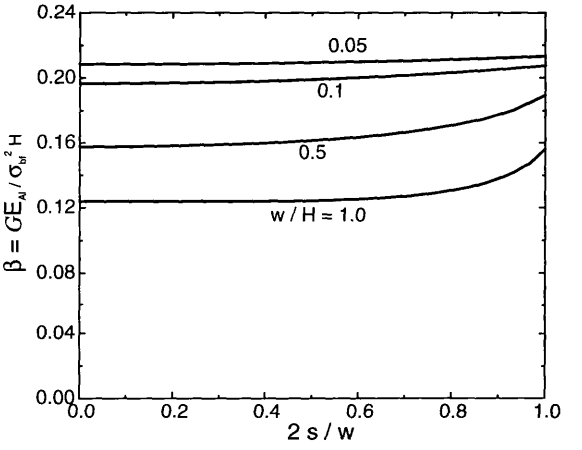

Figure 10. The dimensionless number β for off-center tunneling crack as a function of the crack position s, which is the off-center distance from the middle of trench.

stress at the oxide surface ($x_2/H=1.0$) for some cases, the averaged stress over the film thickness decreases with increasing trench width. This accounts for the decreasing β with increasing w. The complexity in the stress field indicates that, by itself, the stress field is unsuitable to be used in design rules.

Figure 9 shows the effects of pad thickness on the normal stress at the middle plane of the trench. It can be seen that the larger the pad thickness the larger the stress. This contributes to the increasing β with increasing pad thickness. The stress in the oxide at the film/substrate interface is small. However, it increases rapidly from the interface to the surface, where the maximum stress occurs.

The energy release rate obtained for tunneling crack at the middle of the trench is a good approximation to that for off-center cracks. This can be seen from the finite element calculations shown in Figure 10. The dimensionless β is insensitive to the crack position. The slightly larger β at the wall ($2s/W=1$) compared to that at the middle ($s=0$) results from the stress concentration at corners.

It should be noted that high tensile stress arises in the aluminum pads under large cooling. This can cause plastic yielding in aluminum. Take a typical value of 100 MPa for the yield strength. The aluminum pads yield at a temperature drop of 40 K. Here we present the normal stresses in the middle of the trench when the aluminum plasticity is considered. The elastic-perfectly-plastic relation is assumed and the plasticity follows the J_2 flow rule. The normal stresses at several locations in the trench are plotted as a function of temperature drops. In Figure 11, A is for the location at $x_2/H=3/4$, B at $x_2/H=1/2$ and C at $x_2/H=1/4$, respectively. Before the aluminum yields, the stresses increase linearly with the temperature drop. After the yielding the stress close to the surface increases much slower, as indicated by the curve A. In contrast, the stresses at lower location *decreases* with further temperature drop. At the location C the normal stress becomes compressive when the temperature drops by $-\Delta T=100$ K. Therefore,

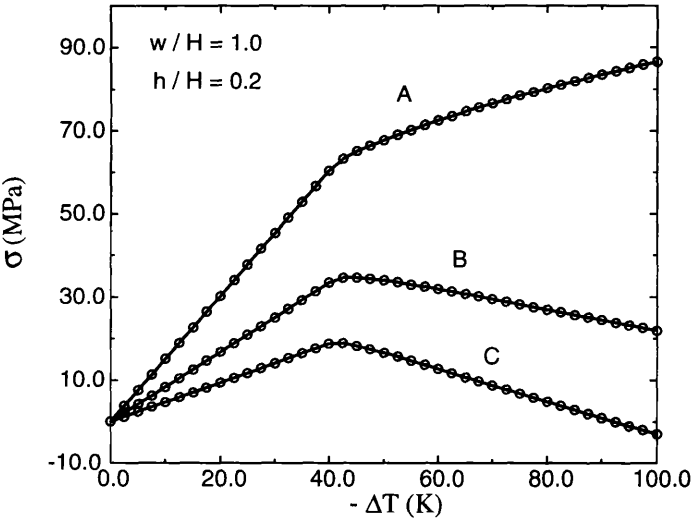

Figure 11. Variations of the normal stress as a function of temperature drop at three locations in the middle of the trench.

the energy release rate has a maximum with respect to temperature drop. Upon cooling from the processing temperature, the structure cracks at some elevated temperature rather than at the room temperature. The effects of plasticity warrant further study.

CONCLUSIONS

Cracking and debonding in integrated microstructures can be avoided by adopting design rules based on fracture mechanics. The design rules hinge on the energy principle that no cracking occurs when the energy release rate is lower than the fracture toughness. One way to avoid cracking in microelectronic structures is to improve the fracture toughness without marring their electrical functions. The other way is to decrease the energy release rate when designing the structures. This is practical because the energy release rate depends strongly on the material properties and the geometry. A third way is to lower the yield stress of the metals. A case study of thermal misfit cracking in multilevel interconnect test structure has been performed. It is shown quantitatively that increasing the trench width or decreasing the aluminum pad thickness can reduce the energy release rate. The design rules are deterministic when the material properties and the geometry are given. They can be incorporated in microelectronic structural designs with other rules regarding electrical functions.

ACKNOWLEDGMENTS

The work was supported by a grant from the Intel Corporation. XHL and ZS were also partly supported by the Institute for Materials Research and Engineering, Singapore. These supports are gratefully acknowledged.

REFERENCES

1. J. Lee, Q. Ma, T. Marieb, A.S. Mack, H. Fujimoto, P. Flinn, B. Woolery, L. Keys, "Measurement and modeling of intrinsic stresses in CVD W lines", in Materials Reliability in Microelectronics V, MRS Proceedings, Vol. **391**, (1995).
2. Q. Ma, J. Lee and H. Fujimoto, "Probing Stresses in Metal Trenches Using Raman Piezospectroscopy" EEP-Vol. **19-1**, in Advances in Electronic Packaging, ASME (1997).
3. B. Greenebaum, A.I. Sauter, P.A. Flinn, and W.D. Nix, Appl. Phys. Lett. **58**, p.1,845 (1991).
4. Y.-L. Shen, S. Suresh, I.A. Blech, J. Appl. Phys. **80**, p.1,388 (1996).
5. I.A. Blech, J. Appl. Phys. **47**, p.1,203 (1976).
6. M.A. Korhonen, P. Borgesen, K.N. Tu, C.-Y. Li, J. Appl. Phys. **73**, p.3,790 (1993).
7. Z. Suo, "Stable state of interconnect under temperature change and electric current", Acta Materialia, in press.
8. Q. Ma, S. Chiras, D.R. Clarke, and Z. Suo, J. Appl. Phys. **78**, 1614 (1995).
9. A. Bagchi, G.E. Lucas, Z. Suo and A.G. Evans, J. Mater. Res. **9**, p.1,734 (1994).
10. Q. Ma, J. Bumgarner, H. Fujimoto, M. Lane, and R. Dauskardt, "Adhesion Measurement of Interfaces in Multilayer Interconnect Structures," in Materials Reliability in Microelectronics VII, MRS Proceedings, Vol. **473**, (1997).
11. Q. Ma, J. Xie, S. Chao, S. El-Mansy, R. McFadden, and H. Fujimoto, "Channeling cracking technique for toughness measurement of brittle dielectric thin films on silicon substrates", in Materials Reliability in Microelectronics VIII, MRS Proceedings, (1998).
12. F.F. Lange, Fracture Mechanics of Ceramics, Vol. **2**, p.599. Plenum, New York, (1976).
13. T.C. Lu, J. Yang, Z. Suo, A.G. Evans, R. Hecht, and R. Mehrabian, Acta Metall. Matter, **39**, p.1,883 (1991).
14. J.W. Hutchinson and Z. Suo, Advances in Applied Mechanics, **29**, p.64 (1991).
15. S. Ho and Z. Suo, Acta Metall. Matter, **40**, p.1,685 (1992).
16. A.G. Evans and J.W. Hutchinson, Acta Materialia, **43**, p. 2,507 (1995).